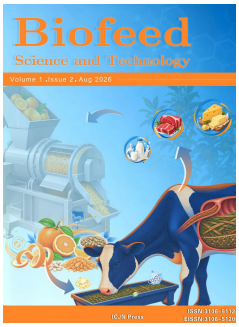
Journal Website: https://www.icjn.net/bst ISSN: 3106-5112 | EISSN: 3106-5120

Biofeed Science and Technology (BST)

ICJN Press Volume. 01 | Issue. 02 | Aug. 2026 DOI: 10.66729/bst202608006



ARTICLE

Efficient Fermentation of *Rhodotorula glutinis* and *Chlorella vulgaris* Composite Feed Additives and Construction of Novel Microcapsule Carriers for Enhancing Carotenoids Stability and Bioaccessibility

Cunyong Qin[1], Jingjing Wu[1], Chi Zhang[2], Tianxiao Li[2], Mengzhuo Yang[2], Shiqi Li[2], Zhiping Zhang[2,*], Lijing Jiao[1,*]

1 Hebei Baisha Tobacco Co., Led., Shijiazhuang Hebei 050011, China.
2 College of Food and Bioengineering, Zhengzhou University of Light Industry, Zhengzhou Henan 450002, China.

*Corresponding Author: Zhiping Zhang, E-mail: zzp@zzuli.edu.cn; Lijing Jiao, E-mail: 156743319@qq.com

Abstract

Mixed-culture products of *Rhodotorula glutinis* and *Chlorella vulgaris* can enhance the antioxidant capacity of target organisms. However, their intrinsic carotenoids exhibit poor stability and bioaccessibility, which hinders the industrial application of related functional feeds. In this study, yeast-algal cells harvested from a 5 L fermenter were double-coated with gelatin and gum arabic. Process parameters were optimized by single-factor experiments and response surface methodology (RSM). Encapsulation efficacy was characterized by zeta potential analysis, Fourier transform infrared (FT-IR) spectroscopy and scanning electron microscopy (SEM). The results showed that the maximum encapsulation rate reached 65.87% at the optimal conditions: wall material concentration of 1.34%, core-to-wall ratio of 58.80%, gelatin proportion in wall materials of 35.40% and curing agent addition of 0.17%. Characterization revealed that re-crystallization-regulated zeta potential facilitated the formation of dense wall structures. Storage stability tests demonstrated enhanced antioxidant retention, and *in vitro* digestion assays verified favorable sustained-release properties. This study effectively improves carotenoid stability and bioaccessibility, providing technical support for high-performance feed additives.

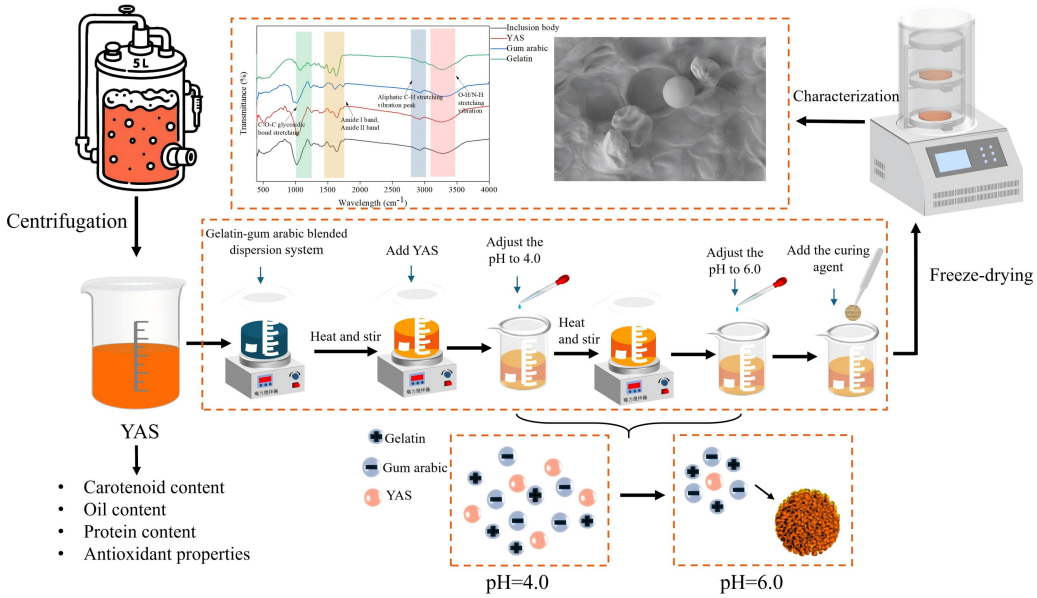
Keywords

Yeast-algal carotenoids; Feed additives; Complex coacervation method; Microencapsulation; Structural characterization

Citation: Cunyong Qin, Jingjing Wu, Chi Zhang, *et al*. Efficient Fermentation of *Rhodotorula glutinis* and *Chlorella vulgaris* Composite Feed Additives and Construction of Novel Microcapsule Carriers for Enhancing Carotenoids Stability and Bioaccessibility. *Biofeed Science and Technology*. 2026, 01 (2): 1-12. doi: 10.66729/bst202608006.

Copyright:© 2026 The Author(s). Published by ICJN Press.
This is an open access article under the https://creativecommons.org/licenses/by/4.0/
Received 8 August 2026; Revised 18 August 2026; Accepted 31 August 2026; Available online 1 September 2026.

Graphical Abstract



NOTE: YAS: yeast-algal slurry. Copyright: PowerPoint 2024.

Highlights

- Developed a co-culture system of *Rhodotorula glutinis* and *Chlorella vulgaris* for efficient carotenoids production.
- Employed a gelatin-gum arabic dual-coating strategy to microencapsulate yeast-algal cells, enhancing carotenoids stability and bioaccessibility.
- Optimized encapsulation parameters via RSM, achieving 65.87% encapsulation rate, surpassing unoptimized processes.
- Demonstrated that zeta potential regulation during recrystallization promotes dense microcapsule formation, validated by FT-IR and SEM.
- The microencapsulated product showed sustained release and improved antioxidant retention during *in vitro* digestion.

1. Introduction

As naturally occurring tetraterpenoid pigments, carotenoids act as vitamin A precursors that can be bioconverted into retinol *in vivo*, and exhibiting strong antioxidant activities such as singlet- oxygen and free-radicals scavenging. In food and feed industries, they exert dual functions in immune enhancement and physiological regulation[1]. Carotenoids have been widely applied in the feed industry to enhance immunity of livestock and poultry and improve flesh color in aquatic animals[2]. However, as a natural pigments, microbial carotenoids face challenges including low yields from single microbial strains and high production costs, limiting their industrial application and scale-up[2]. Furthermore, owing to their highly hydrophobic molecular structure, carotenoids readily undergo isomerization and degradation upon exposure to light, heat, and oxygen, with typical water solubility below 0.01 g/L. Such degradation reduces color intensity, provitamin-A activity, bioaccessibility and bioavailability, thereby impairing their biological functionalitie[3].

Both *Rhodotorula glutinis* and *Chlorella vulgaris* are promising strains for efficient microbial carotenoid production because of their fast growth rates, low cost of substrates, and high yields of products[4,5]. Notably, mixed culture technology developed according to their distinct nutritional requirements has exhibited considerable application potential[2]. This technique facilitates the synthesis and accumulation of high-value-added carotenoids. Nevertheless, improving product stability and extending shelf life remains a major challenge for industrial application. Traditional solutions such as nanoemulsion suspensions [6,7,8] and starch gel encapsulation[9,10,11] improve improve the solubility of target products but suffer from low loading capacities or complex processes. Developing low-cost, highly compatible carrier systems that can physically encapsulate target substances and shield them against environmental stressors holds promise as an effective strategy to overcome the bottlenecks in the application of microbial carotenoids. Microencapsulation technology can fabricate core-shell structures, providing a physical barrier and controlled-release platform for lipophilic functional factors. Existing shell materials include polysaccharides[12] (e.g., oxidized starch, sodium alginate), proteins[13,14] (e.g., whey protein, gelatin), and composite materials[15,16]. This technology offers advantages such as non-toxic raw materials, mild processing conditions, and efficient preservation of the core antioxidant activity, making it promising for encapsulating multi-component bioactive compounds (e.g., carotenoids and lipids) in mixed yeast-algal products.

In this study, mixed yeast-algal cells were successfully cultivated in a 5 L fermenter. Using gelatin and gum arabic as wall materials, microcapsules were fabricated via a composite coagulation method. To optimize the encapsulation process, response surface methodology was adopted to investigate the effects of core-to-wall ratio, wall material ratio, wall material concentration, and curing agent concentration on cell encapsulation rate. Furthermore, the encapsulation performance of the optimized process was comprehensively characterized through zeta potential measurements, Fourier transform infrared (FT-IR)

spectroscopy, and scanning electron microscopy (SEM). The optimized strategy successfully constructed a safe and stable core-shell structure, which balances the encapsulation rate of target substances and the retention of functional activity. Preliminary *in vitro* simulated gastrointestinal digestion tests verified that the microcapsules possessed favorable sustained-release properties. This work provides a feasible technical basis for the development of novel functional feed additives.

2. Materials and Methods

2.1 Yeast-Algal Co-Culture Preparation in 5 L Fermenter and Functional Components Analysis

R. glutinis strain CGMCC No. 2258, which was purchased from the China National Research Institute of Food and Fermentation Industries, was kept on yeast extract, peptone, and dextrose (YEPD) agar slant at 4 ℃. The *C. vulgaris* was provided by Beijing University of Chemical Technology and stored at 4 ℃ on BG-11 agar slants containing glucose (2 g/L), with cell densities of approximately 10^7 cells/mL and 10^6 cells/mL.

Seed media of *R. glutinis* and *C. vulgaris* were consulted to our previous paper[17]. A specific volume of mixed medium was prepared following the formulation method for *C. vulgaris* seed culture medium (BG-11), then adding potassium dihydrogen phosphate to 7 g/L, sodium sulfate to 2 g/L, magnesium sulfate heptahydrate to 1.50 g/L and glucose to 40 g/L. The initial pH value of all media was adjusted to 5.5 and sterilized at 116 ℃ for 30 min. Seed cultures of *R. glutinis* and *C. vulgaris* were used two 500 mL erlenmeyer flasks containing 100 mL seed media, respectively. The shaking (ZQZY-88, Zhichu Instrument, China) speed and temperature were 220 rpm and 30 ℃, and the flasks were exposed to light at an intensity of 4,000 Lux provided by LED lamps. Light intensity was measured by a light-meter (SMART-AR813A, China) on the outside surface of flasks. The monocultures of *R. glutinis* and *C. vulgaris* were cultured to logarithmic growth stage as seed (1 : 1, *v/v*) for a 5 L fermentation tank (BIOSTAT B, Sartorius, Germany). Fermentation conditions in the 5 L fermenter were as follows: 4 L mixed medium, 200 mL seed cultures, fermentation temperature 30 ℃, aeration rate 4 L/min (sterile filtered air), stirring speed 300 r/min. The outside surface of the fermenter was illuminated by LED lamps at 5,000 Lux, and the fermentation was conducted for 7 days. During the 7-day fermentation, the 10 mL samples were withdrawn aseptically every 12 h. Dry cell weight (DCW) was determined by centrifuging a 10 mL sample at 5,000 rpm for 10 min, washing the pellet twice with distilled water, and drying at 105 °C to a constant weight. The growth curve was generated based on these DCW measurements. Distinguishing between these two species in co-culture is technically challenging. Therefore, the presented growth curve reflects the overall DCW of mixed culture. Yeast-algal wet cells were collected by centrifugation (4 ℃, 5,000 rpm) (Centrifuge 5424 R, Eppendorf, Germany) and freeze-dried (FreeZone 4.5 L, Labconco, USA) for future utilization.

With minor modifications based on reference[18], approximately 0.10 g of freeze-dried microbial cells was rehydrated with sterile deionized water. Grind the reconstituted material cells thoroughly in a mortar on ice to break down the cells. 95% (*v/v*) ethanol was added as the extraction solvent at a volume ratio of 1 : 20 (sample : ethanol), followed by extraction in a constant-temperature water bath (HH-S4, AiLang Instrument Co., Ltd., China) at 50 °C for 30 min under static conditions. The mixture was then centrifuged at 4,000 rpm for 25 min, and the supernatant was collected as the crude carotenoid extract. Its absorbance at 482 nm was measured using a UV-Vis spectrophotometer (UV-1900i, Beijing Purkinje General Instrument, China), and the value was substituted into Equation (1) to calculate the carotenoids content. To prevent carotenoids degradation during extraction, the entire process was performed in the dark (using amber glassware and wrapping the water bath with aluminum foil) to minimize oxidation.

$$W_1 = \frac{A \times V \times D}{0.16W} \quad (1)$$

In the equation, A is the sample absorbance value; V is the volume of extraction solvent used (mL); D is the dilution factor of the extract; 0.16 is the extinction coefficient; W is the dry weight of the sample (g).

The lipids content standard curve was established with reference to relevant literature[19], and the regression equation was $Y = 0.4216X + 0.6598$ ($R^2 = 0.9936$), where Y denotes the lipids content (μg/mL) and X denotes the absorbance value. Yeast-algal wet cells were mixed with vanillin-phosphoric acid reagent at a mass-to-volume ratio of 1 : 20 (g : mL) for color development. Following a reaction at room temperature for 20 min, the absorbance was determined at 530 nm, and the lipids content was quantified using a pre-established standard curve.

The Kjeldahl method (Kjeltec 8,400, FOSS, Denmark) was employed with a conversion factor of 6.25, and the results were substituted into Equation (2) to calculate the protein content.

$$X = \frac{(V_1 - V_2) \times c \times 0.01410 \times 6.25 \times 100}{m} \quad (2)$$

In the formula: X represents the protein content in the sample (g/100g); V_1 is the volume of standard hydrochloric acid titrant consumed by the test solution (mL); V_2 is the volume of standard hydrochloric acid titrant consumed by the reagent blank (mL); c is the concentration of the standard hydrochloric acid titrant solution (mol/L); 0.01401 is the mass of nitrogen equivalent to 1 mL of standard hydrochloric acid titrant solution (g); m is the mass of the sample (g); 6.25 is the conversion factor for ammonia to protein; 100 is the unit conversion factor, directly observable in the final calculation formula.

The salicylic acid method[20] was applied for the determination of hydroxyl radical scavenging rate in yeast-algal cells, and the detailed experimental procedures are described as follows: Added 1 mL of reconstituted yeast-algal cells to a test tube. Sequentially added 1 mL each of 6 mol/L $FeSO_4$ aqueous solution and 6 mol/L H_2O_2, mixed thoroughly, and let stand for 10 min at room temperature. Then added 1 mL of 6 mol/L salicylic acid solution. Placed the mixture in a 37 °C constant-temperature water bath for 1 h, then measured the absorbance value A_i at 510 nm using a UV-Vis spectrophotometer. Under identical conditions, prepared a blank control group (A_o) with 1 mL distilled water, 1 mL 6 mol/L $FeSO_4$ solution, 1 mL 6 mol/L H_2O_2, and 1 mL 6 mol/L salicylic acid solution. Prepared a control group (A_j) with 1 mL reconstituted yeast-algal suspension, 1 mL 6 mol/L $FeSO_4$, 1 mL 6 mol/L H_2O_2, and 1 mL distilled water. The hydroxyl radical scavenging rate was calculated using Equation (3).

$$\text{Hydroxyl Radical Scavenging Rate}(\%) = \left(1 - \frac{A_i - A_j}{A_o}\right) \times 100 \quad (3)$$

In the equation, A_o, A_i, and A_j represent the absorbance values (510 nm) of the blank control, the experimental group, and the salicylic acid-free control group, respectively.

Prepared three test tubes as follows: Tube 1 was added 1.50 mL of 2,2-diphenyl-1-picrylhydrazyl (DPPH) solution and 1.50 mL

anhydrous ethanol. Tube 2 was added 1.50 mL of anhydrous ethanol and 1.50 mL sample solution. Tube 3 was added 1.50 mL of DPPH solution and 1.50 mL sample solution. Three tubes were incubated in the dark at room temperature for 30 min. Subsequently, measured the absorbance of each tube at 517 nm, and recorded the values as A_0, A_1 and A_2, respectively. The DPPH radical scavenging rate was calculated by substituting these values into Equation (4).

$$\text{DPPH Radical Scavenging Rate}(\%) = \left(1 - \frac{A_2 - A_1}{A_0}\right) \times 100 \quad (4)$$

2.2 Microcapsule Construction: Single-Factor Experiment for Optimizating Preparation Conditions

The construction method of the microcapsule embedding carrier was adopted with minor modifications based on the literature[21]. Appropriate amounts of gum arabic and gelatin (gelatin proportion, mass ratio 50%) were added as wall materials. The mixture was stirred with an electromagnetic stirrer at 400 r/min and 40 °C for 20 min to obtain a composite wall material system. Subsequently, an appropriate amount (equal to the mass of the wall materials) of yeast-algal slurry (YAS, defined as a 30 g/L dry cell weight suspension of the freeze-dried yeast-algal cells in sterile deionized water) was added to the system, and stirring was continued at 400 r/min for 20 min to form a wall-core dispersion. At 40 °C, a 10% acetic acid solution was added to adjust the dispersion pH to 4.0, and stirring was maintained at 400 r/min for 15 min before cessation. The core temperature of the dispersion was cooled to 15 °C naturally, after which the pH value of dispersion was adjusted to 6.0 using 0.20 mol/L NaOH. Glutamine transaminase (Activity: 100 U/g, mass ratio 0.15%) was added as a curing agent, and the mixture was cured at 15 °C for 3 h. Following curing, the microcapsule dispersion was placed in a refrigerator and precipitated overnight at 2−6 °C. The supernatant was filtered off to collect wet microcapsules, which were then poured into molds for pre-freezing at -20 °C for 24 h. After pre-freezing, the microcapsules were demolded and transferred onto stainless steel sample trays, which were placed in a cold trap for a 40 min pre-freezing treatment prior to vacuum freeze-drying. Finally, the dried microcapsule product was obtained.

This experiment aimed to investigate the effects of four variables on the encapsulation rate of microcapsules, with each variable set at five levels: wall material concentration (0.50%, 0.75%, 1.00%, 1.25%, 1.50%), yeast-algal slurry (YAS) proportion (25%, 33.33%, 50%, 66.67%, 75%), gelatin proportion (25%, 33.33%, 50%, 66.67%, 75%), and curing agent addition amount (0.05%, 0.10%, 0.15%, 0.20%, 0.25%).

After encapsulation, the microcapsule sample was washed with deionized water to remove excess colloid, then diluted 100-fold. The diluted sample was gently mixed using a vortex mixer to ensure uniform dispersion of microcapsules and unencapsulated yeast-algal cells in the suspension. Subsequently, the sample was stained with crystal violet, and the stained cells were counted using a hemocytometer. The number of microcapsules (N_1) and unencapsulated yeast-algal cells (N_2) was recorded separately. Finally, the encapsulation rate was calculated using Equation (5).

$$\text{Embedding Rate } (\%) = \frac{N_1}{N_1 + N_2} \times 100 \quad (5)$$

2.3 Microcapsule Construction: Response Surface Experiment for Optimizing Preparation

Based on the results of the single-factor test, a four-factor, three-level response surface experiment by Design-Expert 13 was carried out, taking wall material concentration, YAS proportion, gelatin proportion, and curing agent concentration as independent variables and microcapsule encapsulation rate as the response value. The levels of each factor are presented in **Table 1**.

Table 1. Experimental design factors and coding level

Level	Factor			
	A（Wall material concentration）/ %	*B*（YAS proportion）/ %	*C*（Gelatin content）/ %	*D*（Curing agent concentration）/ %
-1	0.50	25	25	0.05
0	1	50	50	0.15
1	1.50	75	75	0.25

2.4 Analysis of Microcapsule Formation Mechanisms

2.4.1 Zeta Potential Measurement During Recrystallization

Samples were collected at each stage of the recrystallization process, then diluted to a specified multiple with deionized water to ensure the concentration met the detection requirements. A laser particle size scanner (Mastersizer 3,000, Malvern Panalytical, UK) was used to determine the zeta potential change of the samples, with the detection temperature controlled at 25 °C to avoid temperature interference on the potential results. Each sample was subjected to three parallel experiments, and the average value was taken as the final measurement result to ensure data reliability.

2.4.2 Fourier Transform Infrared Spectroscopy (FT-IR) Analysis

FT-IR (Nicolet IS5, Thermo Scientific, USA) was employed to characterize the chemical structure of key components and the final microcapsule product, so as to verify the interaction between wall materials and core materials. The test samples included pure wall materials (gelatin and gum arabic), pure yeast-algal cells (core material), and freeze-dried microcapsules. All samples were ground with potassium bromide (KBr) at a mass ratio of 1 : 100, pressed into transparent flakes, and scanned within the wavenumber range of 4,000–400 cm^{-1}. The resolution was set to 4 cm^{-1}, and the number of scans was 32 times to ensure the spectral signal-to-noise ratio.

2.4.3 Optical Microscopy Observation

As described in Section 2.2, the dispersion state and basic morphology of microcapsules were recorded.

2.4.4 Scanning Electron Microscopy (SEM) Observation

The freeze-dried microcapsule sample was used for SEM (Sigma 300, ZEISS, Germany) observation to analyze its external morphology and surface structure. Approximately 3 mg of the sample was accurately weighed and fixed on a metal specimen stage using conductive double-sided tape. The excess loose powder on the surface was carefully removed by blowing with a rubber bulb to prevent interference with the observation results.

The sample was then placed in a sputter coater for gold coating (coating thickness of 10−20 nm) to improve its conductivity. Finally, the coated sample was placed in a SEM chamber, and the external morphology of microcapsules was observed under a voltage of 10 kV, with representative areas selected for photographing.

2.5 Antioxidant Activity of Microcapsules and Functional Component Release Rate in *In Vitro* Digestion

Microencapsulated samples and untreated microbial cells (0.5 g each, dry weight) were simultaneously placed in an environmental chamber with controlled conditions: temperature 25 °C, atmospheric pressure 101.325 kPa, and constant white light illumination 2,000 lux. At predetermined storage intervals (0, 3, 6, 9, 12, and 15 days), triplicate samples from each group were collected, and DPPH radical scavenging rate was determined. The retention efficiency of antioxidant components was calculated using Equation (4), and the protective effect of microencapsulation on intracellular antioxidant substances was evaluated by comparing the retention rates between microencapsulated and untreated samples.

Digestive fluids were prepared with slight modifications to the method of Mannai *et al.*[22] Simulated gastric fluid (SGF) preparation: 5 g NaCl and 0.10 g pepsin were placed in a 250 mL volumetric flask, adjusted pH value to 1.50 using 1.50 mol/L HCl, and diluted to 250 mL with distilled water. Simulated intestinal fluid (SIF) preparation: 0.68 g K_2HPO_4, 0.857 g bile salts, and 0.20 g trypsin were placed in a 100 mL volumetric flask, adjusted the pH value to 7.4 using 1 mol/L NaOH, and diluted to 100 mL with distilled water. The sample (microcapsule suspension or unencapsulated microbial cells in deionized water) was mixed with SGF at a volume ratio of 1 : 10 (sample : SGF) and incubated at 37 °C, 150 r/min for 3 h. For the intestinal phase, the entire SGF digest (after 3 h incubation) was transferred and mixed with SIF at a 1:10 (digest: SIF, *v/v*) ratio, without intermediate washing or filtration, to simulate the continuous digestive process. Samples were taken every 30 minutes during the digestion process, and the carotenoid release characteristics were quantified using the analytical method established in Section 2.1. The method for measuring microcapsule carotenoid release was determined using Equation (5).

2.6 Statistical Analysis

Data analysis was performed using IBM SPSS Statistics version 20 (IBM Corp., Armonk, NY, USA) and Design-Expert version 13 (Stat-Ease Inc., Minneapolis, MN, USA). This section describes that all experiments were performed in triplicate, and results are expressed as mean ± standard deviation (SD). For the comparison between optimized and unoptimized processes, an independent t-test was used. Significance was set at $p < 0.05$.

3. Results and Discussion

3.1 Yeast-Algal Co-Culture Preparation in 5 L Fermenter and Functional Components Analysis

Both *R. glutinis* and *C. vulgaris* have become the best strains for effective microbial carotenoids production, and co-cultivation of the two strains showed higher efficiency in biomass and product yield than monoculture[17]. The co-culture of *R. glutinis* and *C. vulgaris* was carried out in a 5 L fermenter to prepare yeast-algal cells. The changes in carotenoids and lipids contents during the mixed fermentation process were shown in **Figure. 1**. All indicators exhibited a typical exponential growth pattern during the initial fermentation phase (0−24 h). The DCW and lipids content increased to 35.20 g/L and 10.20 g/L, respectively, with carotenoids content reaching 30.80 μg/g DCW. This phase closely aligns with the metabolic characteristics of the microbial logarithmic growth phase. During the mid-fermentation stage (24−132 h), biomass growth rate markedly slowed and stabilized as microbial growth entered a stationary phase. At this point, microbial growth was constrained by environmental factors such as nutrient substrate depletion and accumulation of metabolic byproducts. During the late fermentation stage (132−168 h), a slight decrease in biomass was observed, attributed to cell death caused by nutrient depletion and the accumulation of toxic metabolites. Carotenoids and lipids content continued to increase throughout this phase, ultimately reaching their maximum values. To ensure cell integrity while maximizing carotenoid and lipid yields, fermentation could be terminated at 156 h (during the late fermentation phase, prior to significant biomass loss).

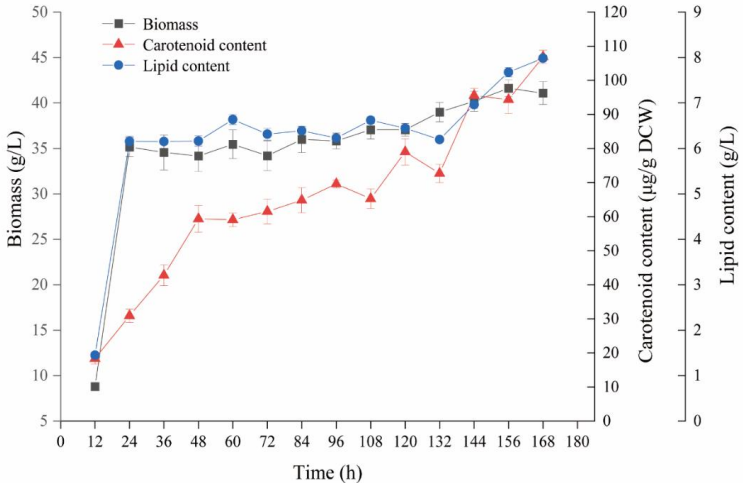


Figure. 1 The preparation of yeast-algal cells and the changes in the content of active ingredients in a 5 L fermenter. Copyright: Origin 2026.

Referring to existing literature on green feed additives[23,24,25], this study found that YAS additives mainly composed of carotenoids have similar effects in terms of lipid content and free radical scavenging ability (**Table 2**). In addition, carotenoids produced through yeast algae intercropping have the characteristics of high concentration, stable yield and safe utilization. In summary, comparative analysis shows that the experimental material in this study is suitable for production as a green and safe feed additive.

Table 2. Comparison of functional and nutritional components of YAS

Ingredients	Protein Content	Fat Content	Free Radical Scavenging Rate	Primary Active Ingredients	References
YAS	24.45%	42.90%	53.02%	Carotenoids	This paper investigates
Mixed Plant Leaf Powder	15.99%	4.48%	24.83%	Phenolic compounds and flavonoids	Falowo *et al.*[23]
Hermetia Illucens Larvae Powder	36.17%	33.84%	——	Crude methanol extract	Geronda *et al.*[24]
Engraulis Japonicus Paste	73.90%	——	49%	Engraulis japonicus paste	Sun *et al.*[25]

3.2 Single-Factor Experiment for Optimizing Preparation Conditions of Microcapsule Construction

Taking the embedding rate of YAS as the evaluation index, single factor experiments were conducted to screen the suitable levels of wall material concentration, YAS proportion, gelatin proportion, and curing agent addition amount. As shown in **Figure. 2(a)**, the embedding rate first increased and then decreased when wall material concentration was in the range of 0.50%−1.50%. The maximum embedding rate was achieved at a wall material concentration of 1%, which was thus determined as the optimal wall material concentration. At excessively low wall material concentrations, the wall material failed to encapsulate all yeast-algal cells, resulting in a significant number of unencapsulated free cells in the system. An increase in the wall material concentration allowed more cells to be encapsulated, thereby improving the embedding rate. However, beyond a certain threshold, further increases in wall material concentration caused the embedding rate to decrease. This occurred because excessively high concentrations elevated solution viscosity, reducing the migration efficiency of gelatin and gum arabic[26], and consequently, these materials failed to distribute uniformly throughout the emulsion system, weakening the encapsulation effect.

As shown in **Figure. 2(b)**, when the YAS proportion was below 50%, the embedding rate increased with the rising YAS proportion. Upon reaching a 50% YAS proportion, the embedding rate peaked. Therefore, 50% is determined as the optimal YAS proportion. At higher YAS proportions (i.e., lower relative wall material content), insufficient wall material led to incomplete encapsulation of the core material, resulting in low embedding rates. Conversely, when the YAS proportion was below 50% (i.e., higher relative wall material content), the significant increase in wall material concentration disrupted the distribution state of wall material molecules in the solution. This, in turn, affected the charge distribution within the system, consequently reducing the embedding rate.

The effect of gelatin proportion on embedding rate is shown in **Figure. 2(c)**. Carrageenan, due to its excellent emulsifying and film-forming properties, significantly impacted the rheological properties of the microencapsulation system as its proportion increased[27]. However, higher carrageenan content reduced the system's dispersibility and fluidity while increasing overall viscosity, making the product prone to caking during drying. Concurrently, increasing the gelatin proportion markedly darkened the color of the finished microcapsules. These results indicated that the wall material ratio was a critical factor influencing the physicochemical properties and encapsulation rate of microcapsules. Experimental data showed that the encapsulation rate peaked when the gum arabic to gelatin ratio reached 1 : 1 (w/w). Thus, this study determined 50% as the optimal gelatin proportion for achieving the best encapsulation effect.

As shown in **Figure. 2(d)**, the microcapsule embedding rate increased with rising curing agent concentration, and reached a maximum at 0.15% (w/v). Therefore, 0.15% was determined as the optimal curing agent concentration. This phenomenon can be attributed to the reversible nature of the recrystallization process. Specifically, the addition of a curing agent facilitates cross-linking reactions among wall material molecules, which effectively suppresses the reversible recrystallization process[28]. Such inhibition of recrystallization enhances the structural stability of the microcapsules, thereby ultimately improving their encapsulation rate. However, excessive curing agent concentration might lead to over-crosslinking of wall materials, resulting in brittle microcapsule structures and a slight decrease in embedding rate.

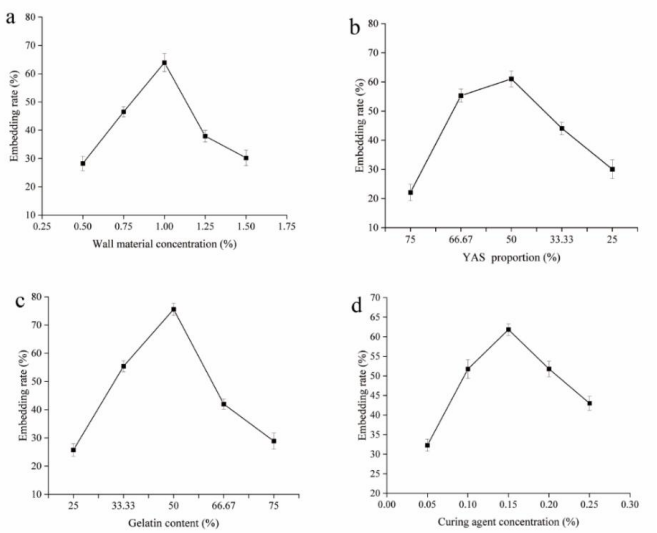


Figure. 2 The influence of different factors on the embedding rate. (a): Effect of wall material concentration on embedding rate; (b): Effect of sample proportion on embedding rate; (c): Effect of gelatin proportion on embedding rate; (d): Effect of curing agent dosage on embedding rate. Copyright: Origin 2026.

3.3 Response Surface Experiment for Optimizing Preparation of Microcapsule Construction

Based on the results of single-factor experiments, four factors were selected: wall material concentration (*A*), YAS proportion (*B*), gelatin proportion (*C*), and curing agent concentration (*D*). The microcapsule encapsulation rate (*Y*) was used as the response value for response surface optimization experiments. The results of the response surface experiments are shown in **Table 3**. Analysis of the data in **Table 3** using Design-Expert 13 yielded the following quadratic polynomial regression equation.

$$Y = 0.7435 - 0.111A + 0.0351B - 0.0042C - 0.0021D + 0.0433AB - 0.0923AC + 0.0293AD - 0.0913BC - 0.0029BD - 0.1196CD - 0.2147A^2 - 0.1660B^2 - 0.1094C^2 - 0.1815D^2$$

Table 3. The response surface analysis of experimental results

Serial Number	*A*	*B*	*C*	*D*	Embedding Rate /%
1	0	-1	-1	0	33.41
2	-1	1	0	0	34.65
3	0	0	0	0	69.73
4	-1	0	0	1	32.74
5	0	0	0	0	74.96
6	0	-1	0	-1	30.11
7	1	0	0	-1	29.95
8	0	1	0	-1	40.69
9	0	0	0	0	79.92
10	1	0	1	0	28.93
11	1	1	0	0	42.06
12	-1	0	0	-1	36.07
13	1	-1	0	0	30.43
14	0	0	1	1	27.99
15	0	0	0	0	71.46
16	-1	0	-1	0	29.59
17	0	-1	0	1	32.20
18	0	0	0	0	70.19
19	0	0	1	-1	57.22
20	0	1	-1	0	59.80
21	-1	-1	0	0	40.36
22	0	-1	1	0	51.19
23	1	0	-1	0	42.92
24	1	0	0	1	38.35
25	0	1	0	1	41.62
26	0	0	-1	1	58.44
27	-1	0	1	0	52.53
28	0	1	1	0	41.04
29	0	0	-1	-1	39.82

The results of analysis of variance (ANOVA) are presented in **Table 4**. As shown in the table, the regression model is highly significant ($p < 0.01$), whereas the lack-of-fit term is not significant ($p = 0.4866 > 0.05$). These findings indicate that the established regression model possesses a strong correlation between the independent variables and the embedding rate, and it can reliably describe the relationship between them. Factors *B*, *AC*, *BC*, *CD*, A^2, B^2, C^2, and D^2 significantly influence the embedding rate ($p < 0.05$). The model yields $R^2 = 0.9596$ and $R^2_{adj} = 0.9193$, indicating that there is a high correlation between predicted and experimental values. The order of influence of factors on sample embedding rate, from greatest to least, is: YAS proportion, wall material concentration, gelatin proportion, and curing agent concentration. The above results indicate that the model can predict the embedding rate well.

Table 4. Analysis of variance for the embedding rate regression model

Sources of Variance	Sum of Squares	Degree of Freedom	Mean Square	*F*	*P*	Significance
Model	0.6653	14	0.0475	23.78	< 0.0001	***
A	0.0015	1	0.0015	0.7377	0.4049	/
B	0.0148	1	0.0148	7.41	0.0166	*
C	0.0002	1	0.0002	0.1076	0.7478	/
D	0.0001	1	0.0001	0.0262	0.8738	/
AB	0.0075	1	0.0075	3.76	0.0730	/
AC	0.0341	1	0.0341	17.06	0.0010	**

Table 4. Analysis of variance for the embedding rate regression model (continued)

Sources of Variance	Sum of Squares	Degree of Freedom	Mean Square	*F*	*P*	Significance
AD	0.0034	1	0.0034	1.72	0.2109	/
BC	0.0334	1	0.0334	16.70	0.0011	*
BD	0.0000	1	0.0000	0.0170	0.8982	/
CD	0.0572	1	0.0572	28.65	0.0001	***
A^2	0.2991	1	0.2991	149.68	< 0.0001	***
B^2	0.1788	1	0.1788	89.48	< 0.0001	***
C^2	0.0776	1	0.0776	38.82	< 0.0001	***
D^2	0.2136	1	0.2136	106.88	< 0.0001	***
Residual	0.0280	14	0.0020	/	/	/
Missing Item	0.0207	10	0.0021	1.15	0.4866	/
Pure Error	0.0072	4	0.0018	/	/	/
Total	0.6933	28	/	/	/	/
	R-squared=0.9596	Adj *R*-squared=0.9193				

NOTE: ***($p < 0.0001$), extremely significant difference; **($p < 0.01$), highly significant difference; *($0.01 < p < 0.05$), significant difference.

As shown in the response surface plot in **Figure. 3**, the effects of all four factors on the embedding rate first increased and then decreased. The three-dimensional response surface further confirms that the interaction surfaces for *AC*, *BC*, and *CD* are steep, indicating that their synergistic effects have a significant impact the embedding rate. The model predicts optimal process parameters as follows: wall material concentration: 1.339%, YAS proportion: 58.824%, gelatin proportion: 35.433%, and curing agent concentration: 0.174%. Under the aforementioned optimal conditions, the predicted encapsulation rate reaches 65.90%. The high coefficient of determination (R^2=0.9596, R^2_{adj}=0.9193) indicates the model can effectively explains embedding rate variations, providing theoretical support for the optimization of the microcapsule preparation process. Based on the above analysis, the response surface regression model provides the optimal process conditions: wall material concentration, YAS ratio, gelatin ratio and curing agent concentration are 1.34%, 58.80%, 35.40% and 0.17%, respectively. To validate the feasibility of the response surface method, experimental verification was conducted under the aforementioned optimal preparation conditions. Three parallel experiments yielded an average encapsulation rate of (65.87 ± 0.52)%.

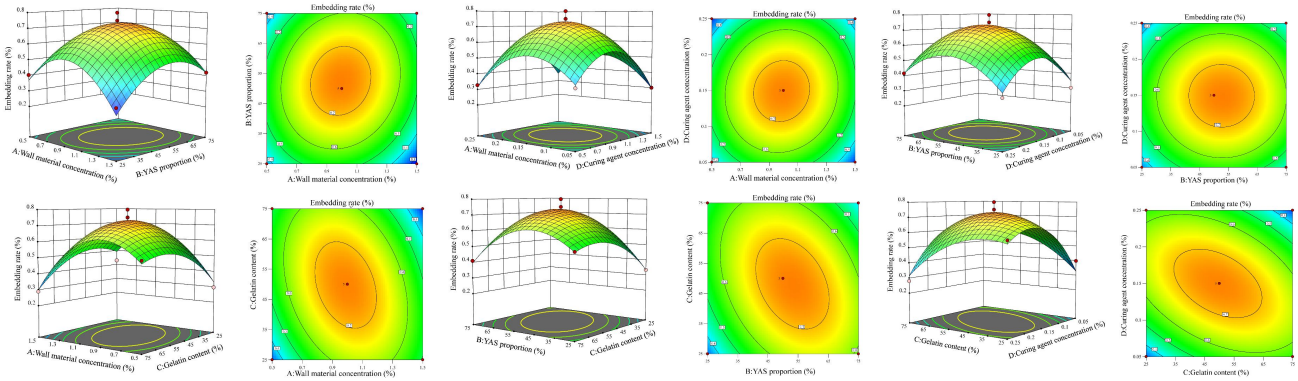


Figure. 3 Response surface and contour diagram of the influence of interaction factors on embedding rate. Copyright: Design-Expert13.

3.4 Mechanism Analysis of Microcapsule Formation

The formation mechanism of YAS microcapsules prepared by the gelatin-gum arabic co-precipitation method relies on the synergistic regulation of molecular interactions and zeta potential. As illustrated in **Figure. 4(a)**, manipulating the system's zeta potential by adjusting pH showed that initially, when the pH was higher than the isoelectric point (pI) of gelatin, both gelatin and gum arabic carried negative charges, which enabled stable emulsification. When the pH decreased below gelatin's pI, the charge of gelatin shifted from negative to positive, generating electrostatic attraction with negatively charged gum arabic. This led to a sharp increase in zeta potential approaching zero, thereby triggering the flocculation and precipitation of a condensed phase that encapsulates the yeast-algal slurry core. This process reconfigures the interaction network at the molecular level, as evidenced by FTIR analysis (**Figure. 4(b)**). Specifically, FTIR results reveal broadened and shifted hydroxyl/amino peaks in the 3000–3500 cm^{-1} region[29], indicating the formation of new hydrogen bond networks between gelatin amino groups and gum arabic carboxyl groups. Additionally, shifts in the amide I/II bands and weakened carboxylate peaks confirm that electrostatic crosslinking modifies the carbonyl environment; weakened aliphatic C-H peaks further suggest the encapsulation of yeast-derived hydrophobic components by the wall materials. Moreover, deformations in glycosidic bond and C-N peaks demonstrate that peptide chains (from gelatin) and polysaccharide chains (from gum arabic) are entangled through hydrogen bonds and other intermolecular interactions. Ultimately, curing results in compact microcapsule structures with a stable, relatively low negative zeta potential. Fundamentally, this process involves potential-driven electrostatic crosslinking, coupled with the synergistic reorganization of hydrogen bonds and hydrophobic interactions, which collectively achieves molecular-level structural reconfiguration and effective encapsulation of yeast-algal components.

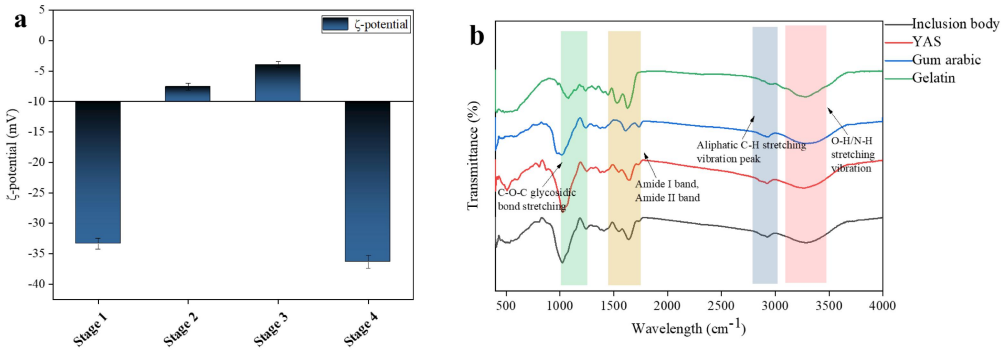


Figure. 4 Zeta potential and infrared spectra analysis of gelatin, gum arabic, yeast-algal cells, and microencapsulated inclusion bodies. (a): Stage 1 (pre-reaction YAS); Stage 2 (recondensation process, pH 4.0); Stage 3 (recondensation process, pH 6.0); Stage 4 (recondensation reaction completed). (b): Infrared spectra of gelatin, gum arabic, unencapsulated of YAS, and microcapsule encapsulations. Copyright: Origin 2026.

Scanning electron microscopy (SEM) was used to observe the surface structural characteristics of microcapsule samples, with the results presented in **Figure. 5**. The results illustrated that the microcapsule particles exhibit intact morphology with uniform spherical geometry. The particle surfaces display no obvious cracks or fissures, further enhancing the microcapsules' ability to protect the encapsulated substances. However, noticeable agglomeration exists between individual microcapsule particles, accompanied by regular depressions on their surfaces. These are typical characteristics of freeze-dried microcapsules, mainly resulting from morphological changes induced by water evaporation during vacuum extrusion and freeze-drying processes[30].

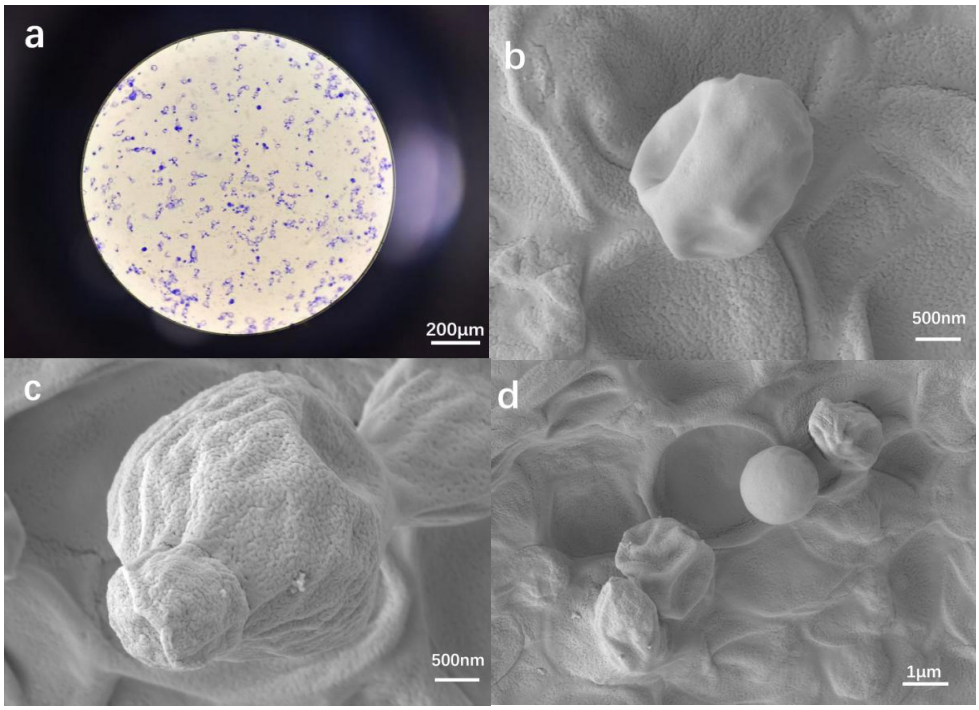


Figure. 5 Morphological observation results of microcapsules. (a): Optical microscope morphology image; (b−d): Scanning electron microscope morphology images. Scale bar: (a): 200 μm; (b−c): 500 nm; (d): 1 μm. Copyright: PowerPoint 2024.

3.5 Antioxidant Capacity and *In Vitro* Digestive Release Rate of Functional Components of Microcapsules

With the aim of clarifying the practical efficacy of microencapsulation technology in enhancing the antioxidant stability of yeast-algal cells, a comparative experiment was designed: microencapsulated samples (experimental group) and untreated yeast-algal cells (control group) were incubated under identical conditions of constant temperature, pressure and illumination, and the dynamic changes in their radical scavenging rates across different exposure periods were monitored. As shown in **Figure. 6**, the antioxidant activity of the control group declined sharply, whereas the experimental group maintained excellent stability, with a smaller decrease in antioxidant activity and a notably higher retention rate. This difference verified that microencapsulation serves as an effective strategy to preserve the antioxidant stability of microbial carotenoids. Notably, microbial carotenoids are natural compounds endowed with significant antioxidant capacities — they can specifically neutralize reactive oxygen species (ROS) produced during biological metabolism, and this ROS-scavenging activity further enables them to shield cells from oxidative stress damage. Therefore, such a protective effect of microencapsulation is thus closely associated with maintaining the structural integrity and functional activity of carotenoids[31]. The results demonstrated that the microcapsule wall material successfully formed a physical

barrier, effectively shielding the microbial carotenoids from degradation by external environmental factors such as oxygen, light, and heat. This significantly slowed the oxidative degradation process, preserved their inherent antioxidant capacity, and thus more effectively maintained the integrity of its molecular structure and biological function.

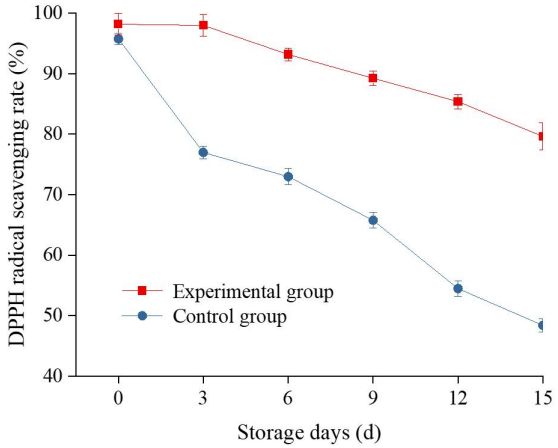


Figure. 6 Preservation of antioxidant properties of yeast-algal carotenoids by microencapsulation. Copyright: Origin 2026.

Figure. 7 demonstrated the sustained-release behavior of carotenoids from encapsulated cells during simulated gastrointestinal digestion. During the gastric digestion phase (SGF environment, 0−180 min), the carotenoid release rate increased gradually over time but remained relatively slow overall. This was attributed to the dense structure of the encapsulation system, which resisted degradation by the low pH environment and pepsin in the stomach, thereby minimizing contact between carotenoids and gastric juices[32]. During the intestinal digestion phase (SIF environment, 210−360 min), both the carotenoid release rate and quantity increased significantly, in contrast to the relatively slow release observed in the gastric phase. This was due to the alkaline intestinal environment and pancreatic enzymes that disrupted the encapsulation carrier structure, leading to substantial release of carotenoids[33]. This "gastric sustained release, intestinal progressive release" pattern demonstrates how encapsulation technology regulates carotenoid release through physical barriers at different gastrointestinal stages. It prevents premature degradation of carotenoids in the stomach while prolonging their release time in the intestines, enhancing the bioaccessibility of carotenoids. Notably, this pattern aligns with the sustained release characteristics of functional components such as Black Tiger anthocyanins and microcapsule core components after encapsulation within the digestive system[34].

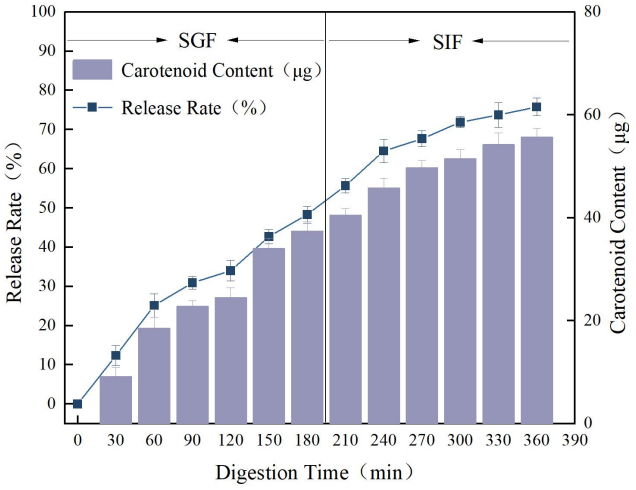


Figure. 7 Changes in carotenoid release rate from microcapsules duringsimulated digestion. Copyright: Origin 2026.

Morphological changes in cells subjected to *in vitro* simulated digestion were visualized under a microscope, and the results were displayed in **Figure. 8**. Before digestion (**Figure. 8(a)**), the cells exhibited intact structures and plump morphology, indicating that cell walls and membrane structures remained intact and could effectively confine intracellular substances such as carotenoids. After 2 h of digestion (**Figure. 8(b)**), the cells exhibited noticeable morphological alterations, including shriveling and collapse, with partial cell wall rupture beginning to occur. This created preliminary conditions for the release of intracellular substances. By 4 h of digestion (**Figure. 8(c)**), cellular structures were severely disrupted, with integrity largely lost, leaving only fragmented remnants. This morphological progression clearly demonstrates that as digestion time increases and digestive activity intensifies, the cell wall is progressively degraded, breaking down the physical barrier. This allows encapsulated liposoluble bioactive compounds, such as carotenoids, to be continuously and extensively released into the digestive environment, thereby enhancing their sustained release characteristics.

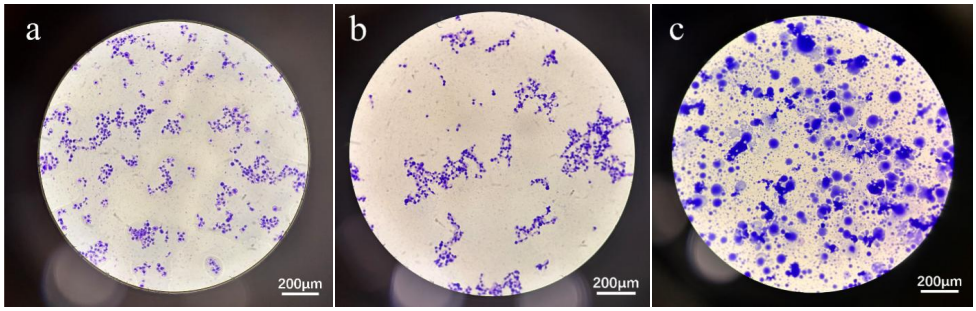


Figure. 8 Microscopic image showing morphological changes in cells undergoing *in vitro* digestion. (a) Undigested cell morphology; (b) Cell morphology after 2 h of digestion; (c) Cell morphology after 4 h of digestion. Scale bar: 200 μm. Copyright: PowerPoint 2024.

4. Conclusions

To address the poor stability and low bioaccessibility of carotenoids (the core active ingredients of yeast-algal feed additives), an efficent microencapsulation strategy was developed for the mixed culture of *R. glutinis* and *C. vulgaris*. Single-factor experiments combined with response surface methodology (RSM) were performed to screen and optimize encapsulation parameters, achieving a maximum encapsulation rate of 65.87%, which was markedly higher than that of the untreated group. Zeta potential analysis, FT-IR spectroscopy, and SEM characterization verified that the gelatin-gum arabic composite wall material formed a compact and integral network structure through recrystallization. This structure enabled effective encapsulation of microbial cells and superior protection of embedded carotenoids. Performance tests demonstrated that the microencapsulated product maintained higher antioxidant activity retention during storage and exhibited desirable sustained-release performance during *in vitro* gastrointestinal digestion. By substantially improving the stability and bioavailability of core bioactive components, the proposed strategy provides both theoretical basis and technical support for the development of high-value, long-acting functional feed additives.

Author Contributions

All authors contributed to the study conception and design. Cunyong Qin and Chi Zhang: writing original draft, method research, data curation. Jingjing Wu: material preparation, date collection, investigation. Tianxiao Li: conceptualization, investigation. Mengzhuo Yang and Shiqi Li: validation, date curation. Zhiping Zhang and Lijing Jiao: writing review & editing, supervision, resources, project administration, funding acquisition, conceptualization.

Funding

This work was supported by the Key R&D Special Project of Henan Province (NO. 241111110400) and the Technology Project of Hebei Baisha Tobacco Co., Ltd. (NO. HBZY2025A043).

Competing Interests

The authors declare that they have no conflict of interests.

Availability of data and materials

Data will be made available on request.

References

[1] Li Z, Li C, Liu H, *et al.* CRISPR-enhanced microalgae biosynthesis: a promising approach for future functional feed ingredients. *Journal of Animal Science and Biotechnology*. 2026, 17 (1): 1-22. [Google Scholar] [CrossRef]

[2] Minaya LQ, Cadena E, Nhu TT, *et al.* Natural pigments in food and feed: Current status, gaps, and sustainability recommendations across biological kingdoms. *Journal of Agriculture and Food Research*. 2026, 29: 1-15. [Google Scholar] [CrossRef]

[3] Neves BV, Ramos SP, Trindade LG, *et al.* Spinning gold: Unraveling the bioaccessibility and bioavailability of Pitanga's carotenoid microfibers. *Food Research International*. 2024, 196:. [Google Scholar] [CrossRef]

[4] Šovljanski O, Beronja M, Saveljić A, *et al.* Microorganisms as biotechnological source of carotenoids. *Natural Products*. 2025, 6 (8): 1-32. [Google Scholar] [CrossRef]

[5] Zhao D, Li C. Effects of TiO_2 and H_2O_2 treatments on the biosynthesis of carotenoids and lipids in oleaginous red yeast *Rhodotorula glutinis* ZHK. *LWT-Food Science and Technology*. 2023, 180: 1-12 [Google Scholar] [CrossRef]

[6] Chang RX, Liu B, Wang QM, *et al.* The encapsulation of lycopene with α-lactalbumin nanotubes to enhance their anti-oxidant activity, viscosity and colloidal stability in dairy drink. *Food Hydrocolloids*. 2022, 131. [Google Scholar] [CrossRef]

[7] Zuo CC, Zhang HJ, Liang S, *et al.* The alleviation of lipid deposition in steatosis hepatocytes by capsaicin-loaded α-lactalbumin nanomicelles via promoted endocytosis and synergetic multiple signaling pathways. *Journal of Functional Foods*. 2021, 79: 1-10. [Google Scholar] [CrossRef]

[8] Du YZ, Bao C, Huang J, *et al.* Improved stability, epithelial permeability and cellular antioxidant activity of β-carotene via encapsulation by self-assembled α-lactalbumin micelles. *Food Chemistry*. 2019, 271: 707-714. [Google Scholar] [CrossRef]

[9] Lei M, Jiang FC, Cai J, *et al.* Facile microencapsulation of olive oil in porous starch granules: Fabrication, characterization, and oxidative stability. *International Journal of Biological Macromolecules*. 2018, 111: 755-761. [Google Scholar] [CrossRef]

[10] Liu YK, Li X, Sun HY, *et al.* Whey protein concentrate/pullulan gel as a novel microencapsulated wall material for astaxanthin with improving stability and bioaccessibility. *Food Hydrocolloids*. 2023, 138. [Google Scholar] [CrossRef]

[11] Sahraeian S, Niakousari M, Fazaeli M, *et al.* Fabrication and study on dually modified starch embedded in alginate hydrogel as an encapsulation system for Satureja essential oil. *Carbohydrate Polymers*. 2023, 322. [Google Scholar] [CrossRef]

[12] Li QY, Liu ML, Liu MJ, *et al.* Preparation, characterization and *in vitro* digestion of jujube polysaccharide microcapsules. *Food and*

Bioproducts Processing. 2024, 145: 97-104. [Google Scholar] [CrossRef]

[13] Daza LD, López SD, Montealegre MÁ, *et al*. Study of the physicochemical properties of hass avocado oil encapsulated by complex coacervation. *LWT-Food Science and Technology*. 2024, 204: 1-10. [Google Scholar] [CrossRef]

[14] He LT, Xu QM, Xin WJ, *et al*. Microencapsulation of *Angelica sinensis* essential oil by complex coacervation using chitosan and gelatin: Optimization, characterization, *in vitro* digestion, and biological activity. *International Journal of Biological Macromolecules*. 2025, 316. [Google Scholar] [CrossRef]

[15] Ahmad K, Ahmad R, Nadia B, *et al*. Marine collagen bio-composites materials: Interactions with small active molecules and their application in food industry. *International Journal of Biological Macromolecules*. 2025, 307. [Google Scholar] [CrossRef]

[16] Sabra R, Roberts CJ, Billa N. Courier properties of modified citrus pectinate-chitosan nanoparticles in colon delivery of curcumin. *Colloid and Interface Science Communications*. 2019, 32. [Google Scholar] [CrossRef]

[17] Zhang ZP, Pang ZJ, Xu SY, *et al*. Improved carotenoid productivity and COD removal efficiency by co-culture of *Rhodotorula glutinis* and *Chlorella vulgaris* using starch wastewaters as raw material. *Applied Biochemistry and Biotechnology*. 2019, 189 (1): 193-205. [Google Scholar] [CrossRef]

[18] Zhou R, Yu X, Ottosen CO, *et al*. Drought stress had a predominant effect over heat stress on three tomato cultivars subjected to combined stress. *BMC Plant Biology*. 2017, 17 (1): 1-13. [Google Scholar] [CrossRef]

[19] Zaldivar J, Nielsen J, Olsson L, *et al*. Fuel ethanol production from lignocellulose: a challenge for metabolic engineering and process integration. *Applied Microbiology & Biotechnology*. 2001, 56 (1): 17-34. [Google Scholar] [CrossRef]

[20] Yu MG, Chen MJ, Gui JL, *et al*. Preparation of *Chlorella vulgaris* polysaccharides and their antioxidant activity *in vitro* and *in vivo*. *International Journal of Biological Macromolecules*. 2019, 137: 139-150. [Google Scholar] [CrossRef]

[21] Dong WX, Guan PY, Liu JG, *et al*. Preparation and characterization of *artemisia argyi* essential oil microcapsule and its application in postharvest preservation of cherry tomatoes. *Food Chemistry*. 2025, 496. [Google Scholar] [CrossRef]

[22] Mannai F, Elhleli H, Abouzied R, *et al*. Encapsulation of sunflower and flaxseed oils using *Opuntia* (Cactaceae) mucilage as a core-shell material through coacervation methods: A study on formulation, characterization, and *in vitro* digestion. *Food Chemistry*. 2024, 459. [Google Scholar] [CrossRef]

[23] Falowo AB, Oloruntola O, Akinmoladun O, *et al*. Assessment of nutritional composition and antioxidant properties of *Dysphania ambrosioides* (L.) *Mosyakin & clemants* and *Crassocephalum crepidioides* leaf meal as potential feed additives. *Turkish Journal of Agriculture-Food Science and Technology*. 2023, 11 (2): 274-279. [Google Scholar] [CrossRef]

[24] Geronda CM, Choresca CH, Pedroso FL, *et al*. Nutritional profile and antibacterial activity of the black soldier fly (*Hermetia illucens*) larvae meal as potential protein source for aquafeeds. *Applied Biochemistry and Microbiology*. 2024, 60 (6): 1375-1387. [Google Scholar] [CrossRef]

[25] Sun J, Su Y, Wang L, *et al*. Nutrients and antioxidant properties of enzymatically hydrolyzed anchovy (*Engraulis japonicus*) paste. *CyTA - Journal of Food*. 2022, 20 (1): 251-258. [Google Scholar] [CrossRef]

[26] Marfil PHM, Paulo BB, Alvim ID, *et al*. Production and characterization of palm oil microcapsules obtained by complex coacervation in gelatin/gum Arabic. *Journal of Food Process Engineering*. 2018, 41 (4). [Google Scholar] [CrossRef]

[27] Glomm WR, Molesworth PP, Yesiltas B, *et al*. Microencapsulation of salmon oil using fish gelatin/gum acacia complexes as wall materials for spray drying: Effect of gelatin source and processing on interfacial tension and oxidative stability. *Food Hydrocolloids*. 2026, 171: 1-10. [Google Scholar] [CrossRef]

[28] Wang KN, Sun H, Cui ZH, *et al*. Synergistic effects of microbial transglutaminase and apple pectin on the gelation properties of pea protein isolate and its application to probiotic encapsulation. *Food Chemistry*. 2024, 439. [Google Scholar] [CrossRef]

[29] Shaddel R, Hesari J, Azadmard-Damirchi S, *et al*. Use of gelatin and gum Arabic for encapsulation of black raspberry anthocyanins by complex coacervation. *International Journal of Biological Macromolecules*. 2018, 107: 1800-1810. [Google Scholar] [CrossRef]

[30] Yang W, Gong YX, Wang YS, *et al*. Design of gum Arabic/gelatin composite microcapsules and their cosmetic applications in encapsulating tea tree essential oil. *RSC Advances*. 2024, 14 (7): 4880-4889. [Google Scholar] [CrossRef]

[31] Tang L, Liu H, Huang G, et al. The structural characterization, physicochemical properties, and stability of gardenia yellow pigment microcapsules. *LWT - Food Science and Technology*. 2022, 162: 1-11. [Google Scholar] [CrossRef]

[32] Zheng JR, Li Y, Lu X, *et al*. Effect of Goji Berry extract on cell viability of *Lactiplantibacillus plantarum* M5 microcapsules during *in vitro* gastrointestinal digestion. *Food Science and Biotechnology*. 2024, 33 (8): 1899-1908. [Google Scholar] [CrossRef]

[33] Raúl E C, Andrea C, Luis C, *et al*. Bioactive *Phaseolus lunatus* peptides release from maltodextrin/gum arabic microcapsules obtained by spray drying after simulated gastrointestinal digestion. *International Journal of Food Science and Technology*. 2019, 54 (6): 2002-2009. [Google Scholar] [CrossRef]

[34] Li YF, Zhang H, Zhao Y, *et al*. Encapsulation and characterization of proanthocyanidin microcapsules by sodium alginate and carboxymethyl cellulose. *Foods*. 2024, 13 (5): 1-19. [Google Scholar] [CrossRef]